Supporting Information

Probing Nanoscale Functionalities of Metal-Organic Framework Nanocrystals

Yao Sun,[a] Zhigang Hu,[b] Dan Zhao,[*b] and Kaiyang Zeng[*a]

[a]Department of Mechanical Engineering, National University of Singapore, 9 Engineering Drive 1, 117576, Singapore

[b]Department of Chemical and Biomolecular Engineering, National University of Singapore, 4 Engineering Drive 4, 117585, Singapore

Correspondence and requests for materials should be addressed to Dr. K.Y. Zeng (E-mail: mpezk@nus.edu.sg) or Dr. D. Zhao. (Email: chezhao@nus.edu.sg).

S1. Materials and Methods

S1.1 Synthesis of NUS-6[1]

All the reagents were obtained from commercial suppliers and used without further purification. The MHT synthesis of NUS-6 was carried out based on our previously reported procedure.[2] Briefly, monosodium 2-sulfoterephtahlic acid (BDC-SO_3Na) (1.3 g, 4.8 mmol) and $ZrCl_4$ (1.2 g, 5.2 mmol) or $HfCl_4$ (1.6 g, 5.0 mmol) dissolved in 50 mL of water/acetic acid (30/20, v/v) mixed solvent were loaded into a flask and heated at 80 °C for 24 h to yield power product of NUS-6. The product was washed with water thrice and soaked in anhydrous methanol for 3 days at room temperature, during which time the extract was decanted and fresh methanol was added every day. After removal of methanol by decanting, the sample was dried under a dynamic vacuum at 150 °C for 24 h to afford the final product. Powder X-ray diffraction (PXRD) patterns were obtained on a Bruker D8 Advance X-ray powder diffractometer equipped with a Cu sealed tube (λ = 1.54178 Å) at a scan rate of 0.02 deg s^{-1}. The XRD pattern is shown on Fig. S1.

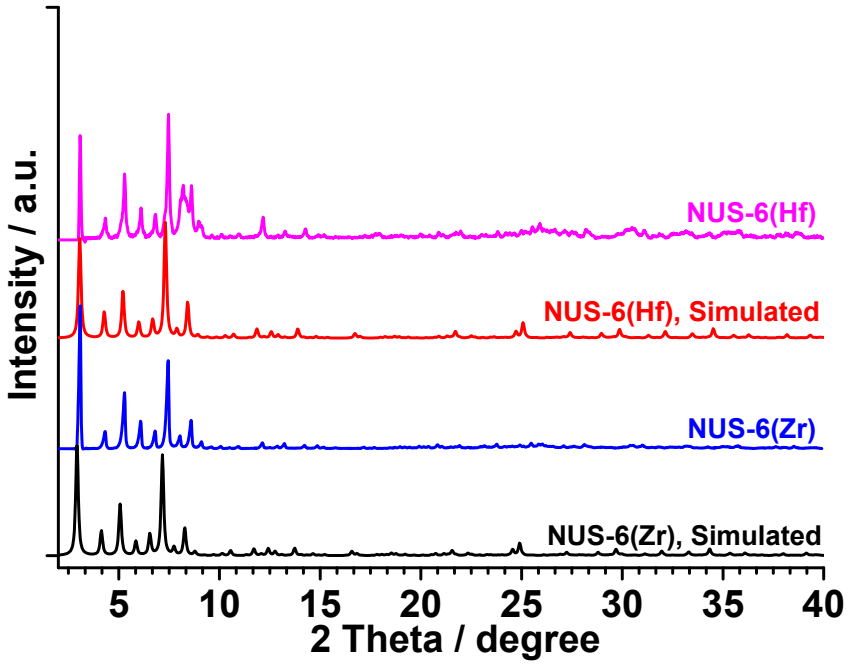

Fig. S1 PXRD patterns of NUS-6.

S1.2 Structure Characterization by SEM

Field-emission scanning electron microscopy (FE-SEM) was conducted on a FEI Quanta 600 SEM (20 kV) equipped with an energy dispersive spectrometer (EDS, Oxford Instruments, 80 mm^2 detector). Samples were treated via Pt sputtering before observation. The surface morphology by SEM is shown in Fig. S2.

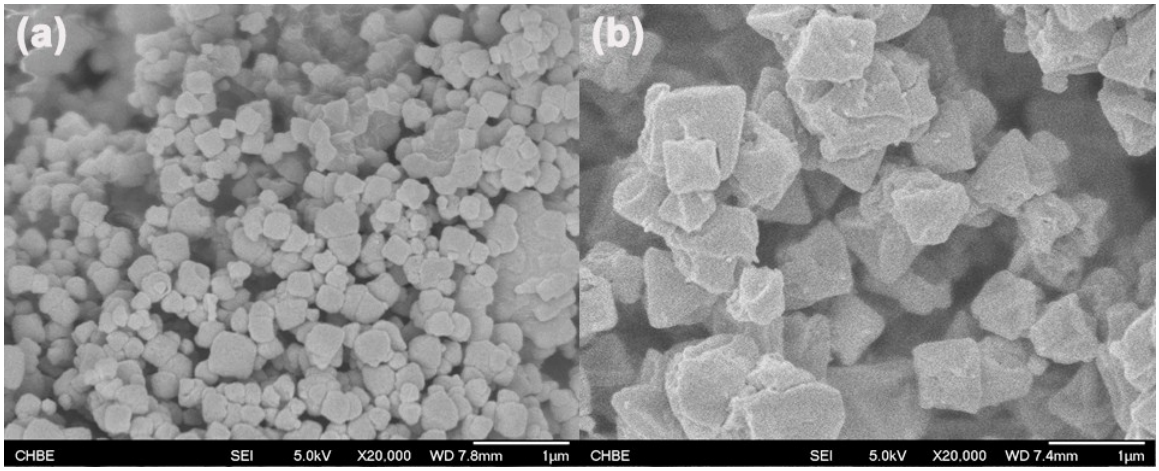

Fig. S2 SEM images of (a) NUS-6-(Zr) and (b) NUS-6-(Hf).

S1.3 Characterization of Functional Property

Dual AC Resonance Tracking Piezoresponse Force Microscopy (DART-PFM) and Piezoresponse Force Spectroscopy (PFS) measurements are conducted using the commercial Scanning Probe Microscopy (SPM, MFP-3D, Asylum Research, CA, USA) were performed to characterize the piezoelectricity and ferroelectricity of NUS-6 MOFs particles respectively. For those measurements, MOFs nanoparticles are suspended in liquid and then are dripped on silicon wafers coated with platinum (Addison Engineering, Inc. CA, USA) and left to dry in air for 24 hours prior to experiments. The conductive AFM probes (AC240TM, Olympus, Japan) are used in both piezoelectricity and ferroelectricity characterization. The detail parameters for this probe are listed in Table S1.

Currently, PFM is the most widely adopted SPM (Scanning Probe Microscopy) method for imaging piezoelectric and ferroelectric materials at nanoscale.[3] This technique is based on monitoring surface

displacement of the piezoelectric sample induced by electric bias using a conductive probe contacted to sample surface all the time. DART[4, 5] is developed which is capable of reducing the crosstalk with topography due to the shift in the resonant frequency during the scanning process, and using a feedback loop to adjust the drive frequency of the cantilever to match the resonance frequencies in different locations. The induced deformation of the probe cantilever is recorded. Fitting the cantilever response by damped (simple) harmonic oscillator (DHO or DSHO) model helps to extract and quantify the sample response. The standard experimental setup of DART-PFM is shown in Fig. S1 and the principle of DHO (DSHO) model available in Supporting Information.

PFS[6, 7] is the technique to acquire the local ferroelectric hysteresis loop from the sample surface. In this technique, the optimal signal-to-noise ratio is achieved at frequencies near the contact resonances of the cantilever. The probe approaches the sample surface in the vertical direction with the deflection set point (trigger force) used as a feedback. When the set point is reached, a hysteresis loop is acquired by sweeping the voltages. During the acquiring process, the conductive probe is fixed at a given location on the sample surface and an electric wave $V_{tip} = V_{dc}(t) + V_{ac}cos\omega t$ is applied to the tip in which the ac voltage V_{ac} is the PFM driving amplitude and the dc voltage $V_{dc}(t)$ is comprised of a sequence of pulses. Usually the responses at dc-off pulses are recorded as amplitude butterfly and phase loops. The ferroelectric hysteresis loop (PR loop) is calculated with the relation of $PR = A \times cos\phi$, where A and ϕ denote amplitude and phase responses respectively. The switching and driving waveform of PFS is presented in Fig. S2.

S1.3.1 Dual AC Resonance Tracking Piezoresponse Force Microscopy (DART-PFM)

PFM is the most widely used scanning probe microscopy (SPM) method for imaging piezoelectric materials and ferroelectrics.[3, 8] This technique is based on monitoring surface displacement of the piezoelectric materials induced by electric bias. A functional generator is used to apply an AC voltage between the tip and the sample surface. The voltage induced deflection of probe cantilever is detected by a reflected laser beam on a four quadrant photodiode.

DART-PFM technique is capable of reducing the crosstalk with topography due to the shift in the resonant frequency, and using a feedback loop to adjust the drive frequency of the cantilever to match the resonance frequency. Rather than using the phase (ϕ) information as the input to the frequency feedback, DART-PFM uses the difference between the two amplitudes as the input feedback. Fig. S3 (b) shows the schematic of the two frequencies, and the resulting amplitudes (A_1 and A_2) when the resonant frequency changes. For example, if the frequency shifts downward, A_1 moves to $A_1^{'}$ and A_2

moves to $A_2^{'}$. The change in the $A_2 - A_1$ signal causes the feedback loop to respond by changing the drive frequency until the $A_2 - A_1$ signal is zero again.[4, 5]

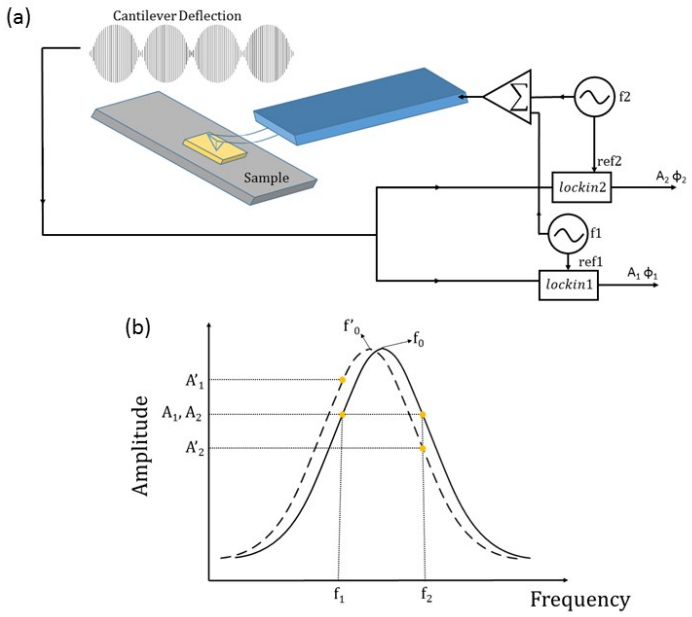

Fig. S3 Standard experimental setup (a) and principle (b) of DART-PFM method. Referring to Gannepalli et al.[4]

S1.3.2 Damped (Simple) Harmonic Oscillator (DHO or DSHO) Model

The obtained responses are directly from the cantilever rather than the sample and the cantilever motion is influenced by the oscillation of sample according to the inverse piezoelectricity. The sample oscillation responses A_{drive} and ϕ_{drive} induced by electric field can be extracted by fitting the responses to the DHO (DSHO) model. The DHO (DSHO) is appropriate for modeling single eigenmode characterization if the tip-sample interaction doesn't significantly perturb the oscillation of the cantilever.[6, 9] In this model, the responses amplitude A_{drive} and phase ϕ_{drive} of cantilever oscillation can be expressed by the formulas.[5]

$$A(f) = \frac{f_0^2 A_{drive}}{\sqrt{(f_0^2 - f^2)^2 + (\frac{f_0 f}{Q})^2}},$$

(S1)

$$\phi(f) = tan^{-1}\frac{f_0 f}{Q(f_0^2 - f^2)} + \phi_{drive} \quad \text{(S2)}$$

By solving these two equations, the sample responses A_{drive}, ϕ_{drive}, contact resonance frequency f and Q factor can be extracted from the four known parameters from the cantilever oscillation A_1, A_2, ϕ_1, ϕ_2. Therefore, the piezoresponse of the sample can be quantified by DART-PFM technique.

S1.3.3 Piezoresponse Force Spectroscopy (PFS)

PFS is the technique to acquire the local ferroelectric hysteresis loop from the sample surface. In this technique, the optimal signal-to-noise ratio is achieved at frequencies near the contact resonances of the cantilever. The tip approaches the sample surface in the vertical direction with the deflection set point (trigger force) used as a feedback. When the set point is reached, a hysteresis loop is acquired by swept the bias.

During the PFS experiment, the tip is fixed at a given location on the sample surface and an electric wave is applied to the tip. The ac voltage V_{ac} is the PFM driving amplitude. The $V_{dc}(t)$ is comprised of a sequence of pulses with amplitude V_i and length τ_1 (high state/dc-on) separated by intervals of zero bias with the duration of τ_2 (low state/dc-off). The envelope for the voltage pulses is specified by a triangular wave having amplitude V_{max} and time periodic T. The waveform of PFS is shown in Fig. S4.

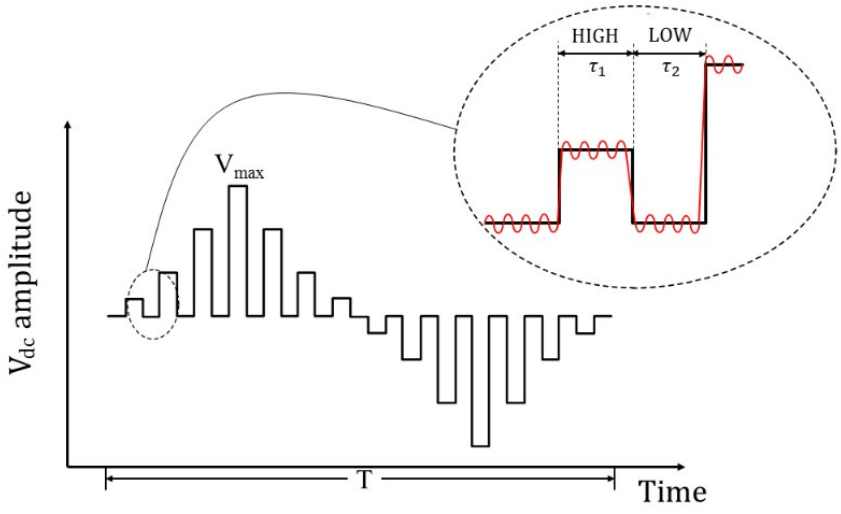

Fig. S4 The switching and driving waveform of PFS.

S1.4 Nanomechanical Property and Thermal Stability Characterization

S1.4.1 Bimodal (Multifrequency) SPM Technique

The dynamic Multifrequency SPM is based on tapping mode and is a new nanomechanical testing method developed in recent years.[10] By simultaneously exciting probe at two or more eigenfrequencies, it can achieve fast imaging of sample topography, elastic or composition information. According to the selection of amplitude modulation (AM) or frequency modulation (FM) at each eigenmode, multifrequency AFM can be divided into AM-AM, AM-FM, FM-FM modes.

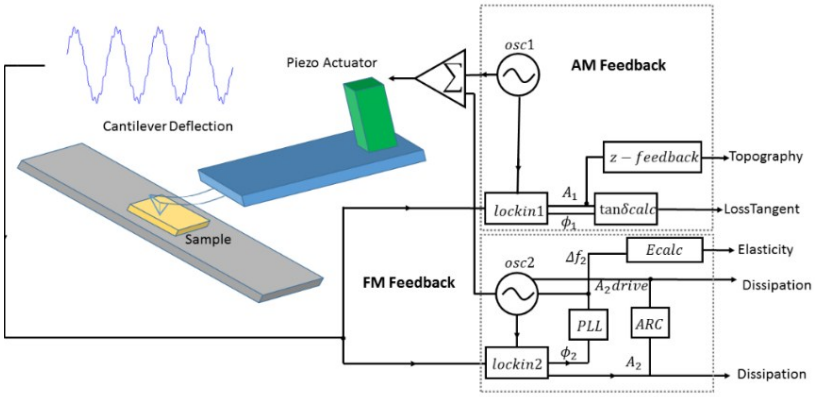

Fig. S5 The specific setup schematics of AM-FM

In our study, AM-FM technique which requires two function generators and two lock-in amplifiers is adopted. The frequencies given by the two function generators are selected at the former two eigenfrequencies, the second mode amplitude (10mV) is generally smaller than the basic mode (2V). The much smaller drive amplitude for second eigenmode is chosen to avoid the perturbation to the basic eigenmode cantilever oscillation. After superimposition of the two frequencies, the signal is put into the piezoelectric ceramics to actuate the cantilever. At the same time, the two signals generated by signal generator are put into the lock-in amplifier as reference signals so as to separate the response signals of the probe. Fig. S5 schematically shows AM-FM setup.

The relationship between tip-sample contact stiffness and second eigenmode frequency shift is[11]

$$k_{ts} \approx 2k_2\Delta f_2/f_2^0, \qquad \text{(S3)}$$

where k_2, $f_2^0$and Δf_2 are the spring constant, second eigenmode resonant frequency and second eigenmode resonant frequency shift. From the Hertz contact theory, the tip-sample contact stiffness can also be written as[11]

$$k_{ts} = 2a_c E^* . \quad \text{(S4)}$$

Where a_c is the tip-sample contact radius. By combining the equations (S3) and (S4), we can obtain the equivalent modulus as:[11]

$$E^* = \frac{k_2 \Delta f_2}{a_c f_2^0} = C\Delta f_2 .$$

(S5)

Because of the uncertainty of contact radius, reference material with a known elastic modulus is usually adopted to calibrate and calculate the elastic modulus of the sample. If the elastic modulus of reference material is proximate to sample, the contact radius of tip-reference material is postulated to be same with tip-sample contact radius. The constant coefficient could be determined by replicating the same experiment and obtaining a relationship between equivalent elastic modulus and second mode contact resonance frequency shift on reference material.

For Hertz contact model, the contact stiffness between tip and sample is a first derivative of applied pressure to deformation which can be written as:

$$k^* = \frac{\delta F_N}{\delta \delta} = \sqrt[3]{6E^{*2} R F_N} . \quad \text{(S6)}$$

where δ, F_N, and R are the deformation, applied force and tip radius, respectively. If single reference material is adopted, the relationship between contact stiffness and equivalent elastic modulus could be obtained from equation (S6).

$$E_{s-tip}^{*} = E_{ref-tip}^{*}\left(\frac{\frac{k_{s-tip}^{*}}{k_c}}{\frac{k_{ref-tip}^{*}}{k_c}}\right)^{n}, \quad \text{(S7)}$$

where E_{s-tip}^{*}, $E_{ref-tip}^{*}$, k_{s-tip}^{*}, $k_{ref-tip}^{*}$ and k_c are tip-sample equivalent elastic modulus, tip-reference material equivalent modulus, tip-sample contact stiffness, tip-reference material contact stiffness and cantilever spring constant, respectively. As for Hertz contact model, n=3/2. And E_{s-tip}^{*} can be written as:

$$E_{s-tip}^{*} = \frac{1}{M_s} + \frac{1}{M_t} \quad \text{(S8)}$$

where M_t and M_s are the elastic modulus of the tip and sample. Substituting equations (S8) into (S7), the elastic modulus of the sample can be obtained.

$$M_s = \left\{\left[\left(\frac{\frac{k_{ref-tip}^{*}}{k_c}}{\frac{k_{s-tip}^{*}}{k_c}}\right)^{3/2}/M_{ref}\right] + \left[\left(\frac{\frac{k_{ref-tip}^{*}}{k_c}}{\frac{k_{s-tip}^{*}}{k_c}}\right)^{3/2} - 1\right]/M_t\right\}^{-1}. \quad \text{(S9)}$$

S1.4.2 Characterization of Temperature-dependent Mechanical Property

The dynamic Multifrequency SPM is based on tapping mode SPM. By simultaneously exciting probe at two or more eigenfrequencies, it can achieve fast imaging of sample topography, elastic or composition information. In our work, first amplitude tapping mode in topography imaging combined

with second mode frequency modulation in elasticity imaging AM-FM technique was adopted. The specific setup schematics (Fig. S5) and principle of AM-FM are available in Supporting Information. In this technique, tip-sample equivalent modulus can be derived from tip-sample contact stiffness, and then a proper reference sample is required to accomplish the calculation of elastic modulus from equivalent modulus. For this measurement, the nonconductive AFM probe AC160TS (Olympus, Japan) with spring constant of 35N/m was adopted. Specific experimental parameters including the cantilever dimension, first and second resonant frequencies, inverse optical lever sensitivity are listed in Table S1. A wafer of pure Magnesium (40GPa) (Fig. S6) was chosen as reference sample to calculate MOFs' elastic modulus. By introducing the heating stage (Polyheater^{TM}, Asylum Research, CA, USA) to AM-FM tests, elastic modulus of the NUS-6(Hf) and NUS-6(Zr) nanocrystals at a series of temperatures (298K, 333K, 363K) are measured.

All of the SPM based experiments are conducted under the ambient air condition with the relative humidity of 50-60%.

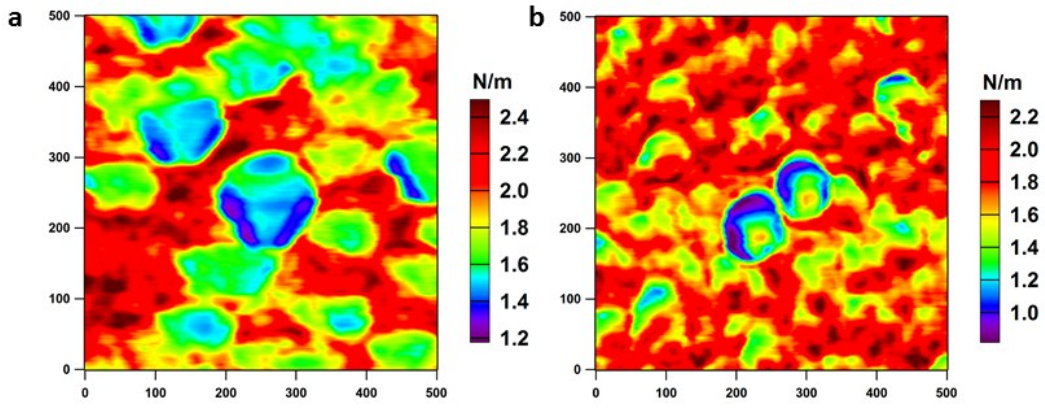

Fig. S6 Tip-sample contact stiffness images of (a) NUS-6-(Hf) and NUS-6-(Zr).

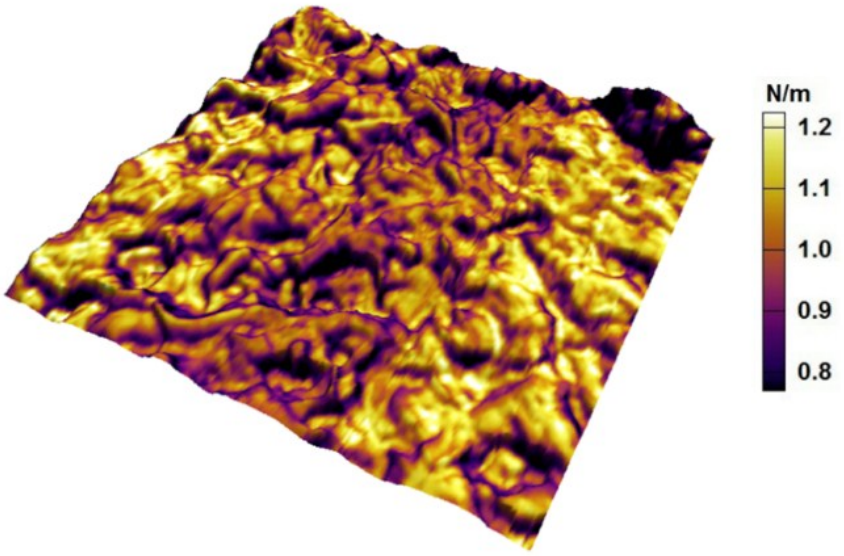

Fig. S7 AM-FM 3D image of pure Magnesium (Mg), stiffness overlay on topography.

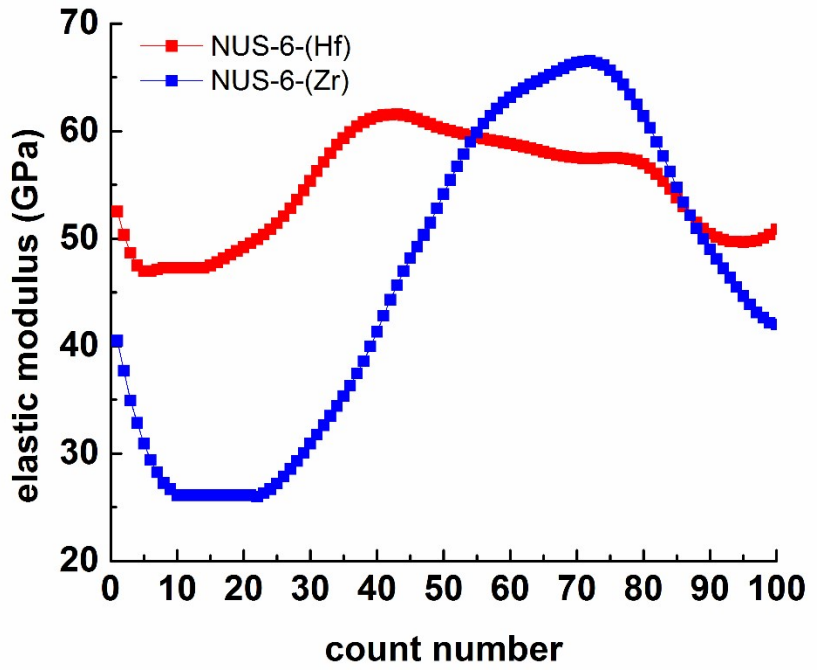

Fig. S8 AM-FM elastic modulus along the line profile across particle in the SPM images (Figs. 4c and 4d in main text) of the NUS-6-(Hf) and NUS-6-(Zr).

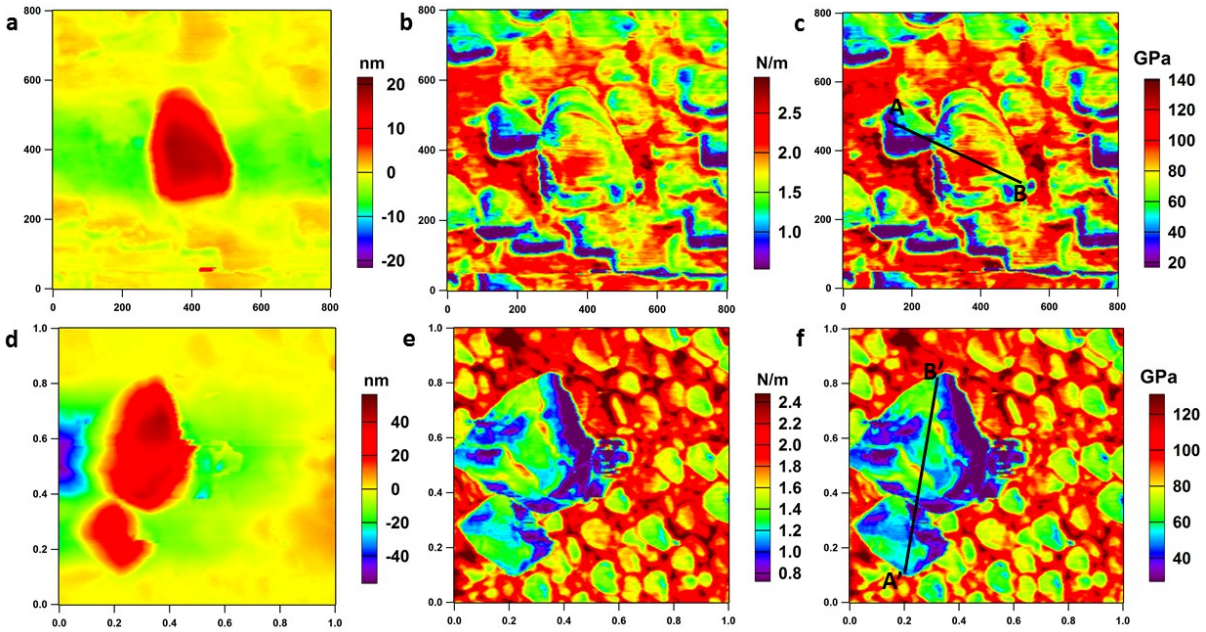

Fig. S9 AM-FM topography (1st column), stiffness (2nd column) and elastic modulus (3rd column) images of NUS-6-(Hf) (1st row) and NUS-6-(Zr) (2nd row) particles.

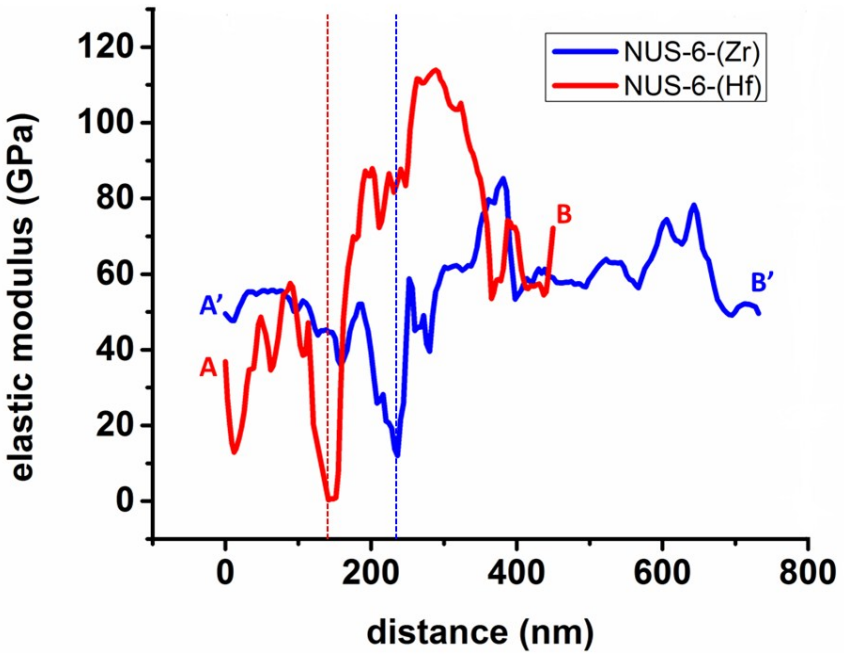

Fig. S10 AM-FM elastic modulus along the line profile across particles in the SPM images (Figs. S9c and S9f) of the NUS-6-(Hf) and NUS-6-(Zr). The dash lines indicate the particle boundaries of the two NUS-6-(Hf) and NUS-6-(Zr) particles.

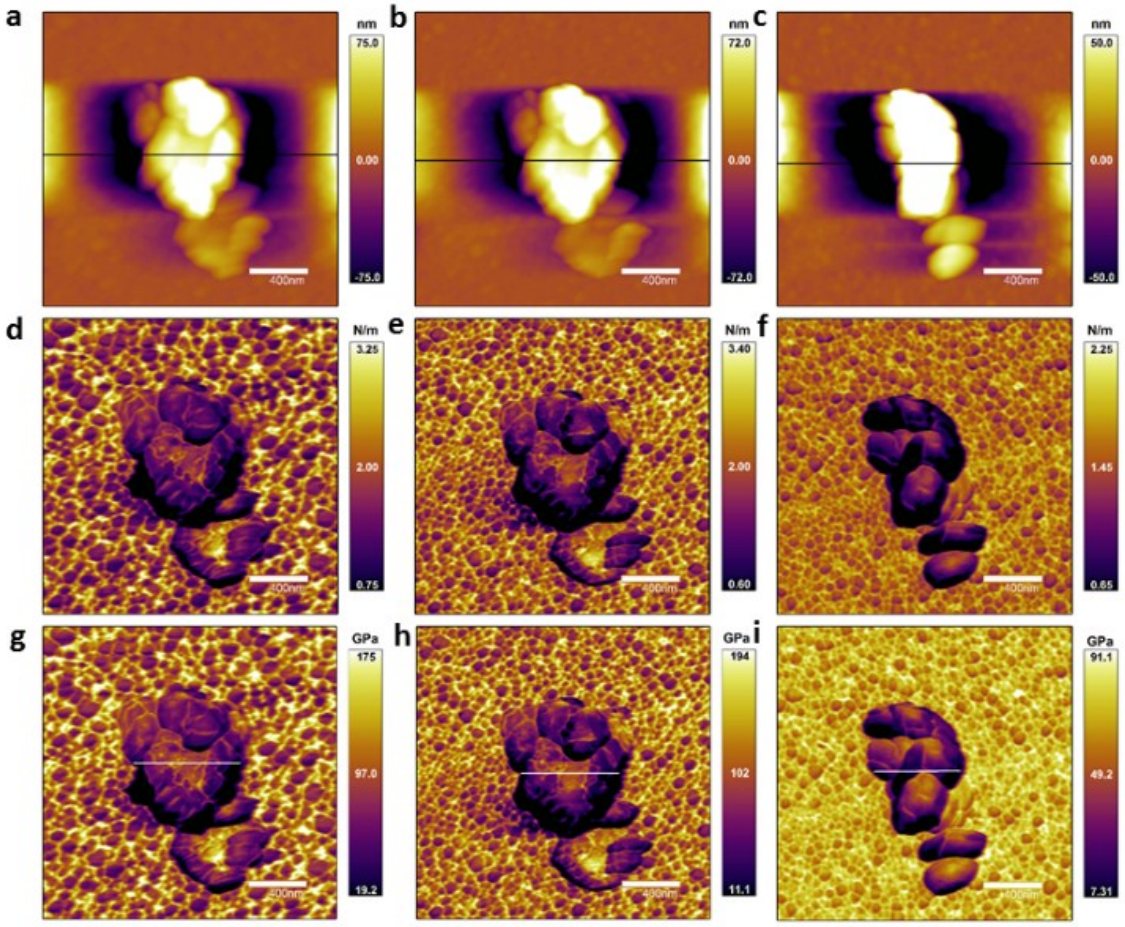

Fig. S11 AM-FM topography (1st row), stiffness (2nd row) and elastic modulus (3rd row) images on same single particle of NUS-6-(Hf) at 298K (1st column), 333K (2nd column) and 363K (3rd column).

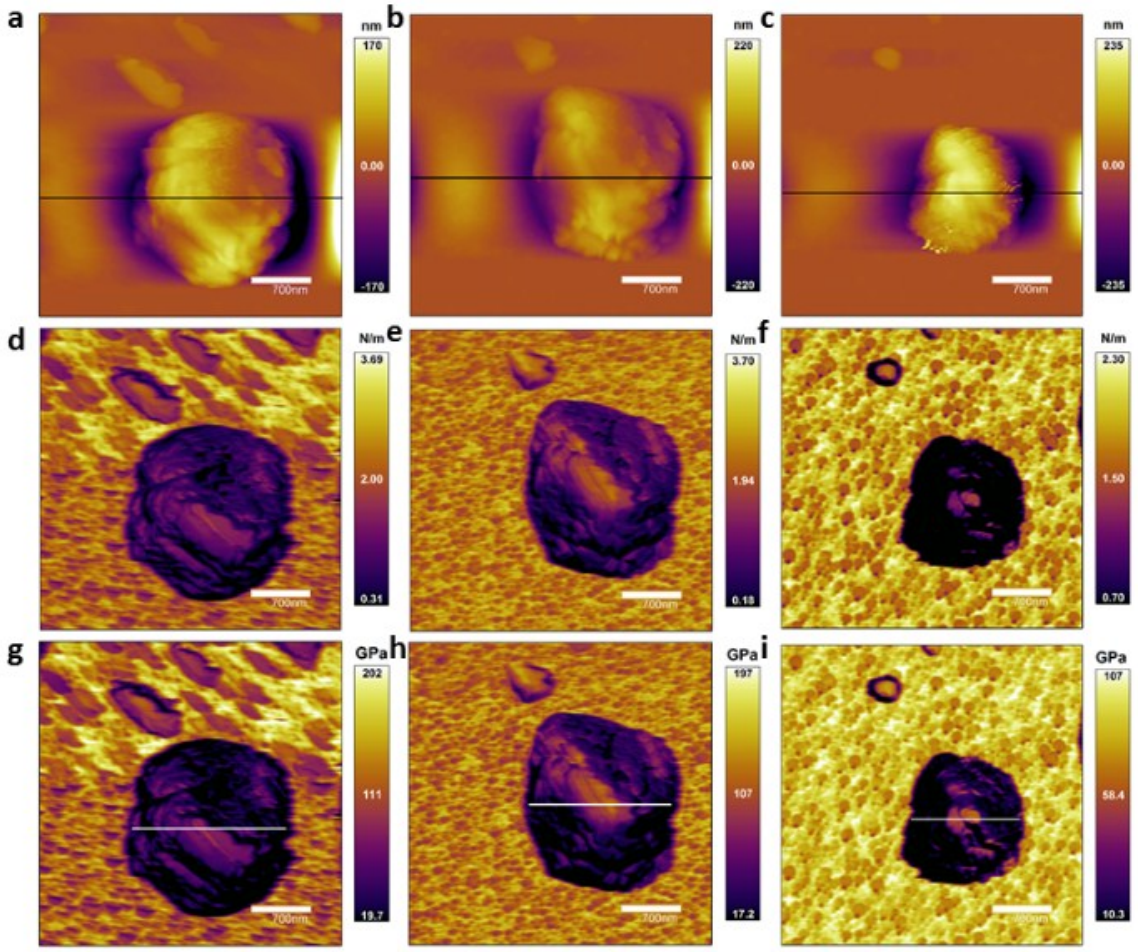

Fig. S12 AM-FM topography (1st row), stiffness (2nd row) and the elastic modulus (3rd row) images on same single particle of NUS-6-(Zr) at 298K (1st column), 333K (2nd column) and 363K (3rd column).

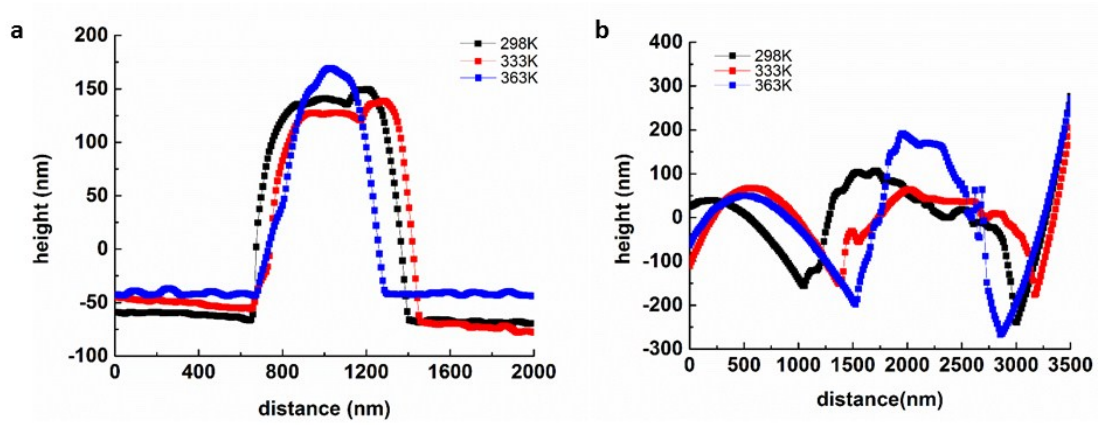

Fig. S13 Height line-profile in topography images of NUS-6-(Hf) and NUS-6-(Zr) in Fig. S9, S10.

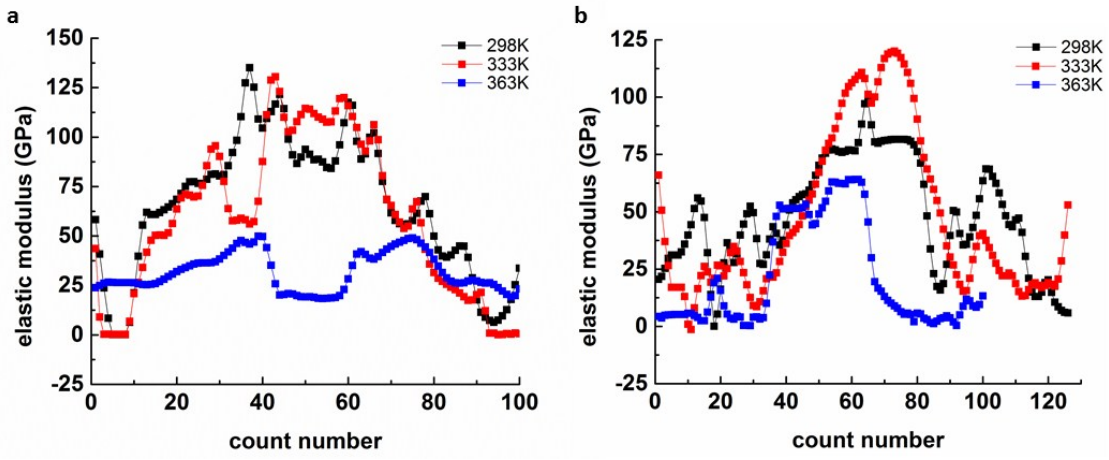

Fig. S14 Modulus line-profile in elastic modulus images of NUS-6-(Hf) and NUS-6-(Zr) in Fig. S9, S10.

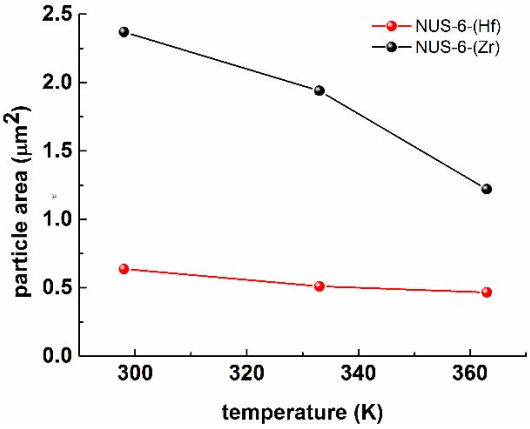

Fig. S15 Particle areas of NUS-6-(Hf) and NUS-6-(Zr) at function of temperature.

Table S1. Experimental specifications of SPM probe (240AC-PP)

Specifications	**Values**
First eigenmode resonant frequency, kHz	70
Second eigenmode resonant frequency, kHz	390
First eigenmode stiffness k, N/m	0.6~3.9
Cantilever dimension (L, W, H), µm	240, 40, 2.6
Tip radius of curvature, nm	25±10
Coating (tip and cantilever)	Pt

Table S2. Experimental specifications of SPM probe (AC160TS)

Specifications	**Values**
First eigenmode resonant frequency, kHz	300
Second eigenmode resonant frequency, MHz	1.67
First eigenmode stiffness k, N/m	33~37
Cantilever dimension (L, W, H), µm	160, 40, 3.7
Tip radius of curvature, nm	8±2
Coating (tip and cantilever)	None

Reference

1. Z. Hu, Y. Peng, Y. Gao, Y. Qian, S. Ying, D. Yuan, S. Horike, N. Ogiwara, R. Babarao, Y. Wang, N. Yan and D. Zhao, *Chem. Mater.*, 2016, **28**, 2659-2667.
2. Z. G. Hu, Y. W. Peng, Z. X. Kang, Y. H. Qian and D. Zhao, *Inorg. Chem.*, 2015, **54**, 4862-4868.
3. A. L. Kholkin, S. V. Kalinin, A. Roelofs and A. Gruverman, *Springer New York*, 2007.
4. A. Gannepalli, D. G. Yablon, A. H. Tsou and R. Proksch, *Nanotechnology*, 2011, **22**, 355705.
5. A. Gannepalli, D. G. Yablon, A. H. Tsou and R. Proksch, *Nanotechnology*, 2013, **24**, 159501.
6. V. K. Sergei, N. M. Anna, C. Long Qing and J. R. Brian, *Reports on Progress in Physics*, 2010, **73**, 056502.
7. S. Jesse, H. N. Lee and S. V. Kalinin, *Review of Scientific Instruments*, 2006, **77**, 073702.
8. A. L. Kholkin, S. V. Kalinin, A. Roelofs and A. Gruverman, *Springer New York*, 2007, **173**.
9. S. V. Kalinin, B. J. Rodriguez, S. Jesse, J. Shin, A. P. Baddorf, P. Gupta, H. Jain, D. B. Williams and A. Gruverman, *Microscopy and Microanalysis*, 2006, **12**, 206-220.
10. R. Garcia and E. T. Herruzo, *Nat Nano*, 2012, **7**, 217-226.
11. R. Garcia and R. Proksch, *Eur. Polym. J.*, 2013, **49**, 1897-1906.